TIME DISCRETIZATIONS OF ANISOTROPIC ALLEN–CAHN EQUATIONS

CARSTEN GRÄSER, RALF KORNHUBER, AND ULI SACK

Abstract. We consider anisotropic Allen–Cahn equations with interfacial energy induced by an anisotropic surface energy density γ. Assuming that γ is positive, positively homogeneous of degree one, strictly convex in tangential directions to the unit sphere, and sufficiently smooth, we show stability of various time discretizations. In particular, we consider a fully implicit and a linearized time discretization of the interfacial energy combined with implicit and semi-implicit time discretizations of the double-well potential. In the semi-implicit variant, concave terms are taken explicitly. The arising discrete spatial problems are solved by globally convergent truncated nonsmooth Newton multigrid methods. Numerical experiments show the accuracy of the different discretizations. We also illustrate that pinch-off under anisotropic mean curvature flow is no longer frame invariant, but depends on the orientation of the initial configuration.

1. Introduction

Anisotropic mean curvature flow of a surface Γ with normal $\mathbf{n}$ is characterized by the steepest descent of the anisotropic surface energy

$$\int_\Gamma \gamma(\mathbf{n})\, d\Gamma$$

with respect to the Finsler metric associated with the anisotropy function γ [4]. Note that classical mean curvature flow is recovered for the Euclidean distance $\gamma = |\cdot|$. Driven by a wide range of practical applications in, e.g., metallurgy, crystal growth, or geometry processing, many numerical schemes for the resulting geometric evolution equations have been analyzed, implemented and tested. These schemes cover, e.g., the case of graphs [9, 10], curve shortening flow [12], curves with triple junctions [2], manifolds in higher dimensions [3], or even two dimensional surfaces in higher codimension [24].

In their pioneering paper, Bellettini and Paolini [4] used formal asymptotics to show that anisotropic mean curvature flow can be approximated by anisotropic versions of the Allen–Cahn equation, as obtained by L^2 gradient flow of the anisotropic Ginzburg–Landau energy

$$\mathcal{E}(u) = \int_\Omega \frac{\varepsilon}{2}\gamma(\nabla u)^2 + \frac{1}{\varepsilon}\Psi(u)\, dx.$$

Here, u is an order parameter taking values in some interval, say $[-1, 1]$, and Ψ is a double-well potential that gives rise to phase separation. The surface Γ is then approximated by a diffuse interface of width $\varepsilon > 0$ along the zero level set of u. For

The authors want to thank Gerd Dziuk for continuous encouragement and stimulating discussions. This work was supported by the DFG research center Matheon.

existence, uniqueness, and rigorous convergence proofs, we refer, e.g., to [1, 14, 15] and the literature cited therein.

While the analysis of anisotropic Allen–Cahn equations has reached a certain degree of maturity, anisotropic phase-field computations still seem to be in their infancy. For example, in spite of the parabolic nature of Allen–Cahn equations, fully explicit schemes are frequently used to avoid strongly nonlinear spatial problems to be solved in each time step [5, 6, 17, 23]. Deckelnick et al. [11] suggested a semi-implicit variant where the gradient term is taken implicitly, but no numerical computations or comparisons are included.

In this paper, we analyze, implement, and compare two implicit time discretization schemes. In the *nonlinear* time discretization the anisotropic gradient terms are taken fully implicitly, while in the *linearized* version they are replaced by an isotropic bilinear form weighted by a certain positive factor λ. Further variants are obtained by discretizing the double-well potential ψ either fully implicitly or semi-implicitly. Here, semi-implicit discretization means that only the convex part of ψ is taken implicitly and the concave part is not. Imposing suitable conditions on the anisotropy γ, we prove stability of all variants. It turns out that stability involving a fully implicit discretization of ψ only holds on suitable time step constraints while semi-implicit versions are unconditionally stable.

On one hand the nonlinear semi-implicit scheme is unconditionally stable and involves no further parameters, while stability of the linearized version requires a careful selection of the weighting factor λ. On the other hand both the nonlinear and the linearized schemes require the solution of large-scale, (possibly nonsmooth) nonlinear algebraic systems in each time step. To this end, we use truncated nonsmooth Newton methods (TNNMG) as developed and analyzed in [18, 19, 20].

In our numerical experiments, we first compare the accuracy of all time discretization schemes, using a simple 2D model problem with known extinction time. We observe that for a Kobayashi anisotropy the linearized time discretization is comparable with the nonlinear version, if the weighting factor λ is suitably chosen. For a regularized ℓ^1-norm, however, the linearized scheme fails to produce any useful results. It also turns out that, once the stability constraints on the time step are met, fully implicit discretizations of ψ are typically much more accurate than semi-implicit versions. Comparing the complexity of our time discretizations, it seems that, using our TNNMG solvers, the gain in cpu time by the linearized version is less than expected. It was less than a factor of 3 for the considered model problem. In a final 3D example, we illustrate that occurrence of pinch-off for anisotropic Allen-Cahn flow strongly depends on the orientation of the initial configuration.

2. Continuous problem

2.1. **Anisotropic Ginzburg–Landau free energy.** Let $\Omega \subset \mathbb{R}^d$, $d = 1, 2, 3$, be a domain with Lipschitz boundary. We consider the Ginzburg–Landau free energy

$$\mathcal{E}(u) = \int_\Omega \frac{\varepsilon}{2}\gamma(\nabla u)^2 + \frac{1}{\varepsilon}\Psi(u)\, dx \tag{2.1}$$

with given interface parameter $\varepsilon > 0$, anisotropy function γ, and double-well potential Ψ. The potential Ψ takes the form

$$\Psi(u) = \Phi(u) + \tfrac{1}{2}(1 - u^2) \tag{2.2}$$

with a lower semicontinuous and proper convex function $\Phi : \mathbb{R} \to \mathbb{R} \cup \{+\infty\}$ such that $\phi : H^1(\Omega) \to \mathbb{R} \cup \{+\infty\}$ defined by

$$\phi(v) = \int_\Omega \Phi(v(x))\, dx, \qquad v \in H^1(\Omega), \tag{2.3}$$

is lower semicontinuous and proper convex on $H^1(\Omega)$. Furthermore Φ and thus ϕ is bounded from below by a constant. For simplicity we assume $\Phi(u) \geq 0$. The logarithmic potential $\Phi = \Phi_\theta$,

$$\Phi_\theta(v) = \chi_{[-1,1]}(v) + \frac{\theta}{2}\big((1+v)\log(1+v) + (1-v)\log(1-v)\big), \tag{2.4}$$

and the obstacle potential

$$\Phi_0(v) = \chi_{[-1,1]}(v) \tag{2.5}$$

are typical examples. Here $\chi_{[-1,1]}$ denotes the characteristic function of $[-1,1]$ and $\theta \in [0,1)$ is the normalized temperature. For a proof of the lower semicontinuity of the logarithmic potential we refer to [19]. Regarding the anisotropy function $\gamma : \mathbb{R}^d \to \mathbb{R}$ we make the following assumptions.

(A1) The function $\gamma : \mathbb{R}^d \to \mathbb{R}$ is continuous on $\mathbb{R}^d$, twice continuously differentiable on $\mathbb{R}^d \setminus \{0\}$, positively homogeneous of degree one, i.e.

$$\gamma(\alpha x) = \alpha\gamma(x) \qquad \forall \alpha > 0,\ x \in \mathbb{R}^d \setminus \{0\},$$

and satisfies $\gamma(x) > 0$ for $x \in \mathbb{R}^d \setminus \{0\}$.

(A2) There exists a constant $\gamma_0 > 0$, such that

$$\langle \gamma''(x)y, y\rangle \geq \gamma_0 |y|^2 \quad \forall y, x \in \mathbb{R}^d \text{ with } \langle y, x\rangle = 0 \text{ and } |x| = 1.$$

Here and in the following $\langle \cdot, \cdot \rangle$ denotes the Euclidean scalar product $\langle x, y\rangle = \sum_{j=1}^d x_j y_j$ in $\mathbb{R}^d$ with associated norm $|\cdot|$, and we use the notation

$$\gamma'(x)_j = \frac{\partial \gamma}{\partial x_j}(x), \qquad \gamma''(x)_{ij} = \frac{\partial^2 \gamma}{\partial x_i \partial x_j}(x), \qquad i, j = 1, \dots, d,$$

for the gradient and the Hessian matrix of γ. We note some immediate consequences.

Lemma 2.1. *For $x \in \mathbb{R}^d \setminus \{0\}$ and $\alpha > 0$ there holds*

$$\gamma'(\alpha x) = \gamma'(x), \qquad \gamma''(\alpha x) = \frac{1}{\alpha}\gamma''(x),$$
$$\langle \gamma'(x), x\rangle = \gamma(x), \qquad \gamma''(x)\, x = 0.$$

Together with (A2) this implies

$$\langle \gamma''(x)y, y\rangle \geq 0 \qquad \forall y \in \mathbb{R}^d, x \in \mathbb{R}^d \setminus \{0\}$$

and thus convexity of γ. For the stability estimates we will not need these properties directly but their implications for γ^2.

Lemma 2.2. *The functional $\gamma^2 : \mathbb{R}^d \to \mathbb{R}$ is continuously differentiable on $\mathbb{R}^d$ and twice continuously differentiable on $\mathbb{R}^d \setminus \{0\}$.*

Proof. By the differentiability assumption on γ and the chain rule, γ^2 is twice continuously differentiable on $\mathbb{R}^d \setminus \{0\}$. By

$$\frac{\gamma^2(hx) - \gamma^2(0)}{h} = h\gamma^2(x) \xrightarrow[h\searrow 0]{} 0 \qquad \forall x \in \mathbb{R}^d \setminus \{0\}$$

we get $(\gamma^2)'(0) = 0$ while continuity of $(\gamma^2)'$ in 0 follows from $|(\gamma^2)'(x)| \le C|x|$ with suitable $C > 0$. □

Lemma 2.3. *The Hessian $(\gamma^2)''(x)$ of γ^2 is positive definite for $x \in \mathbb{R}^d \setminus \{0\}$.*

Proof. For $x \neq 0$ the Hessian $(\gamma^2)''$ of γ^2 is given by

$$(\gamma^2)''(x) = 2\gamma'(x)^T\gamma'(x) + 2\gamma(x)\gamma''(x).$$

Now let $y \neq 0$ with $y = \alpha x + x^\perp$ for some $\alpha \in \mathbb{R}$ and $\langle x, x^\perp \rangle = 0$. If $x^\perp = 0$ we have

$$\langle (\gamma^2)''(x)y, y\rangle = 2\alpha^2 |\langle \gamma'(x), x\rangle|^2 + 2\alpha^2\gamma(x)\langle \gamma''(x)x, x\rangle = 2\alpha^2\gamma(x)^2 > 0.$$

Otherwise we have

$$\langle (\gamma^2)''(x)y, y\rangle = 2|\langle \gamma'(x), y\rangle|^2 + 2\gamma(x)\langle \gamma''(x)x^\perp, x^\perp\rangle \ge 2\gamma_0\gamma(x)|x^\perp|^2 > 0.$$

Hence $(\gamma^2)''(x)$ is symmetric and positive definite for all $x \neq 0$. □

It was shown in [16, Remark 1.7.5] that positive definiteness of $(\gamma^2)''$ is even equivalent to Assumption (A2) provided that γ satisfies Assumption (A1).

As an immediate consequence of Lemma 2.3, the Hessian of γ^2 induces a uniformly equivalent norm on $\mathbb{R}^d$.

Lemma 2.4. *There are constants $\mu, L > 0$ such that the Hessian of γ^2 satisfies*

$$\mu|y|^2 \le \langle (\gamma^2)''(x)y, y\rangle \le L|y|^2 \qquad \forall x \in \mathbb{R}^d \setminus \{0\}, y \in \mathbb{R}^d.$$

Proof. Using the continuity of $(x, y) \mapsto \langle (\gamma^2)''(x)y, y\rangle \in \mathbb{R}$ on the compact set $S^{d-1} \times S^{d-1}$ we find that the constants

$$L = \sup_{x,y\in S^{d-1}} \langle (\gamma^2)''(x)y, y\rangle, \qquad \mu = \inf_{x,y\in S^{d-1}} \langle (\gamma^2)''(x)y, y\rangle > 0 \tag{2.6}$$

provide the assertion. □

Lemma 2.5. *The gradient $(\gamma^2)' : \mathbb{R}^d \to \mathbb{R}^d$ is Lipschitz continuous with Lipschitz constant L.*

Proof. Let $x, y \in \mathbb{R}^d$. If 0 is not contained in the line segment $[x, y] = \mathrm{co}\{x, y\}$ then γ^2 is twice continuously differentiable on $[x, y]$ and we can use the fundamental theorem of calculus and boundedness of the Hessian from above to obtain

$$|(\gamma^2)'(x) - (\gamma^2)'(y)| \le L|x - y|.$$

Utilizing this estimate on the line segment $[\delta x, y]$ for $\delta > 0$ and the continuity of $(\gamma^2)'$ we let $\delta \to 0$ to establish Lipschitz continuity on $[0, y]$. If $0 \in [x, y]$ we have $y = \alpha x$ for some $\alpha \le 0$ and thus

$$\begin{aligned} |(\gamma^2)'(y) - (\gamma^2)'(x)| &\le |(\gamma^2)'(y) - (\gamma^2)'(0) + (\gamma^2)'(0) - (\gamma^2)'(x)| \\ &\le L\Big(|y - 0| + |0 - x|\Big) = L|y - x| \end{aligned}$$

by $|x| + |y| = (1 - \alpha)|x| = |x - y|$. □

Note that we had to take special care about the case $0 \in [x, y]$ since $(\gamma^2)'$ is not differentiable in 0 and we do not know a priori if the fundamental theorem of calculus can be applied in this case.

Lemma 2.6. *The gradient $(\gamma^2)' : \mathbb{R}^d \to \mathbb{R}^d$ is strongly monotone. More precisely we have*

$$\big\langle (\gamma^2)'(y) - (\gamma^2)'(x), y - x \big\rangle \geq \mu |y - x|^2 \qquad \forall x, y \in \mathbb{R}^d.$$

Proof. Let $x, y \in \mathbb{R}^d$. If 0 is not contained in the line segment $[x, y]$ we can again use the fundamental theorem of calculus and boundedness of the Hessian from below to obtain

$$\big\langle (\gamma^2)'(y) - (\gamma^2)'(x), y - x \big\rangle \geq \mu |y - x|^2.$$

Again, a continuity argument can be used to extend estimate to the case $x = 0$ or $y = 0$. If $0 \in [x, y]$ we have $y = \alpha x$ for some $\alpha \leq 0$ and thus

$$\begin{aligned}
&\big\langle (\gamma^2)'(y) - (\gamma^2)'(x), y - x \big\rangle \\
&\quad = \Big\langle (\gamma^2)'(y) - (\gamma^2)'(0) + (\gamma^2)'(0) - (\gamma^2)'(x), y - x \Big\rangle \\
&\quad = \frac{\alpha - 1}{\alpha} \Big\langle (\gamma^2)'(y) - (\gamma^2)'(0), y - 0 \Big\rangle + (1 - \alpha) \Big\langle (\gamma^2)'(0) - (\gamma^2)'(x), 0 - x \Big\rangle \\
&\quad \geq \mu \Big(\frac{\alpha - 1}{\alpha} |y|^2 + (1 - \alpha) |x|^2 \Big) = \mu \Big(|y - x||y| + |y - x||x| \Big) = \mu |y - x|^2.
\end{aligned}$$

□

Here we used similar techniques as in Lemma 2.5 to deal with the case $0 \in [x, y]$. As an alternative we could have also applied the fundamental theorem of calculus directly, because it is already clear that $(\gamma^2)'$ is Lipschitz continuous and thus absolutely continuous.

As a direct consequence we get the strong convexity of γ^2.

Corollary 2.1. *The functional $\gamma^2 : \mathbb{R}^d \to \mathbb{R}$ is strongly convex. More precisely we have*

$$\gamma^2(x) - \gamma^2(y) \geq \Big\langle (\gamma^2)'(y), x - y \Big\rangle + \frac{\mu}{2} |x - y|^2 \qquad \forall x, y \in \mathbb{R}^d.$$

Strong convexity and Lipschitz continuity of the derivative of γ^2 are both directly inherited by the smooth part $\mathcal{J}_0 : H^1(\Omega) \to \mathbb{R}$ of the Ginzburg–Landau free energy given by

$$\mathcal{J}_0(u) := \frac{\varepsilon}{2} \int_\Omega \gamma^2(\nabla u)\, dx. \tag{2.7}$$

The derivative $\nabla \mathcal{J}_0(u) \in H^1(\Omega)'$ at $u \in H^1(\Omega)$ reads (see, e.g., [19])

$$\langle \nabla \mathcal{J}_0(u), v \rangle = \frac{\varepsilon}{2} \int_\Omega \big\langle (\gamma^2)'(\nabla u), \nabla v \big\rangle \, dx = \varepsilon (\gamma(\nabla u) \gamma'(\nabla u), \nabla v).$$

Here and in the following, the brackets $\langle \cdot, \cdot \rangle$ are also used for he dual pairing of $H^1(\Omega)$ and $H^1(\Omega)'$ while $(\cdot, \cdot)$ stands for the usual scalar product in $L^2(\Omega)$ generating the L^2-norm $\| \cdot \|_0$.

Corollary 2.2. *The functional $\mathcal{J}_0 : H^1(\Omega) \to \mathbb{R}$ is strongly convex with respect to the semi-norm $\|\nabla \cdot\|_0$, i.e.,*

$$\mathcal{J}_0(u) - \mathcal{J}_0(v) \geq \langle \nabla \mathcal{J}_0(v), u - v\rangle + \frac{\varepsilon\mu}{4}\|\nabla u - \nabla v\|_0^2 \qquad \forall u, v \in H^1(\Omega).$$

Corollary 2.3. *The gradient of the functional $\mathcal{J}_0 : H^1(\Omega) \to \mathbb{R}$ is Lipschitz continuous with respect to the semi-norm induced by the semi-norm $\|\nabla \cdot\|_0$, i.e.,*

$$\sup_{\substack{w\in H^1(\Omega)\\ \|\nabla w\|_0=1}} |\,\langle \nabla \mathcal{J}_0(u) - \nabla \mathcal{J}_0(v), w\rangle\,| \leq \frac{\varepsilon L}{2}\|\nabla u - \nabla v\|_0 \qquad \forall u, v \in H^1(\Omega).$$

Due to homogeneity, anisotropy functions are characterized by their Frank diagram $F_\gamma = \{x \in \mathbb{R}^d \mid \gamma(x) \leq 1\}$. While F_γ illustrates deviations from the isotropic case in the energy, the Wulff shape $W_\gamma = \{x \in \mathbb{R}^d \mid \gamma^*(x) \leq 1\}$ involving the polar functional $\gamma^*(y) = \sup_{x\in\mathbb{R}^d\setminus\{0\}} \langle x, y\rangle / \gamma(x)$ gives the energetically favored phase shape (Wulff's Theorem) [8, 25]. We refer to [4, 11, 24] for further information and conclude this section by two examples of anisotropy functions γ satisfying our assumptions (A1) and (A2).

Example 2.1 (Kobayashi)**.** *In his pioneering paper Kobayashi [22] introduces the anisotropy*

$$\gamma_{k,\bar a} : \mathbb{R}^2 \to \mathbb{R}, \qquad \gamma_{k,\bar a}(x) = \begin{cases} (1 + \bar a \cos(k\beta(x)))\,|x| & ,\ x \neq 0 \\ 0 & ,\ x = 0 \end{cases} \tag{2.8}$$

where $k \in \mathbb{N}$, $\bar a > 0$ and $\beta(x) \in [0, 2\pi]$ is the angle between x and the (positive) horizontal axis. Assumption (A1) *is obviously satisfied. Moreover, $(\gamma_{k,\bar a}^2)''$ is positive definite for $\bar a < \bar a_c := \frac{1}{k^2-1}$ (see [7]) so that (A2) again follows from [16, Remark 1.7.5]. Figure 2.1 illustrates the Frank diagram and the Wulff shape of $\gamma_{3,0.124}$.*

Example 2.2 (Regularized ℓ^1-norm)**.** *Another example is a smooth approximation of the ℓ^1-norm given by*

$$\gamma_{\mathtt{E}}(x) = \sum_i \sqrt{x_i^2 + \mathtt{E}|x|^2} \tag{2.9}$$

for $\mathtt{E} > 0$. Verification of (A1) *and* (A2) *is straightforward. Figure 2.1 illustrates the Frank diagram and the Wulff shape of $\gamma_{\mathtt{E}}$ for $\mathtt{E} = 10^{-3}$.*

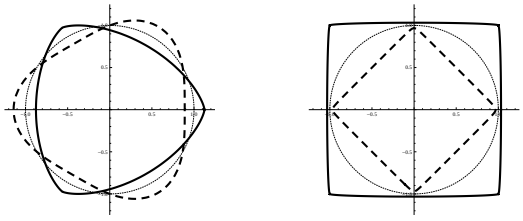

FIGURE 2.1. Frank diagram (thick dashed), Wulff shape (thick) and Euclidean 1-sphere (thin dashed) for $\gamma_{k,\bar a}$ with $k = 3$, $\bar a = 0.124$ (left) and $\gamma_{\mathtt{E}}$ with $\mathtt{E} = 10^{-3}$ (right)

2.2. **Anisotropic Allen–Cahn equation.** Denoting

$$\mathcal{E}(u) = \mathcal{J}_0(u) + \frac{1}{\varepsilon}\psi(u), \qquad \psi(u) = \int_\Omega \Psi(u(x))\,dx = \phi(u) + \frac{1}{2}\left(|\Omega| - \|u\|_0^2\right), \tag{2.10}$$

according to (2.1), (2.2), and (2.3), the anisotropic Allen–Cahn equation

$$\varepsilon(u_t, v-u) + \langle \nabla \mathcal{J}_0(u), v-u\rangle + \frac{1}{\varepsilon}\big(\phi(v)-\phi(u)\big) - \frac{1}{\varepsilon}(u, v-u) \geq 0 \tag{2.11}$$

is obtained as L^2-gradient flow of the scaled Ginzburg–Landau free energy $\mathcal{E}/\varepsilon$. For the logarithmic potential (2.4), the variational inequality (2.11) can be rewritten as a semilinear parabolic differential equation which degenerates to a differential inclusion for the obstacle potential as $\theta \to 0$. Of course, (2.11) has to be completed by an initial condition $u^0 \in L^\infty(\Omega)$ with $|u^0(x)| < 1$ almost everywhere. In the case of a smooth function Φ, existence and uniqueness of a weak solution $u \in L^2(0,T;H^1(\Omega)) \cap L^\infty(\Omega \times (0,T))$ is stated by Alfaro et al. [1].

3. Nonlinear time discretization

3.1. **Fully implicit nonlinear Euler method.** Let $T > 0$ and let $\tau = T/M$ with fixed $M \in \mathbb{N}$ be a uniform time step. Starting from the given initial condition u^0, we determine approximations $u^m \in H^1(\Omega)$ at $t_m = m\tau$, $m = 1, \dots, M$, from the spatial problems

$$\begin{aligned} u^m \in H^1(\Omega): \quad & \frac{\varepsilon}{\tau}(u^m - u^{m-1}, v-u^m) + \langle \nabla \mathcal{J}_0(u^m), v-u^m\rangle \\ & + \frac{1}{\varepsilon}\big(\phi(v)-\phi(u^m)\big) - \frac{1}{\varepsilon}(u^m, v-u^m) \geq 0 \qquad \forall v \in H^1(\Omega). \end{aligned} \tag{3.1}$$

We emphasize that (3.1) can be equivalently rewritten as the minimization problem

$$u^m \in H^1(\Omega): \qquad \mathcal{J}(u) \leq \mathcal{J}(v) \qquad \forall v \in H^1(\Omega)$$

for the energy functional

$$\begin{aligned} \mathcal{J}(v) &= \mathcal{J}_0(v) + \frac{1}{\varepsilon}\phi(v) + \Big(\frac{\varepsilon}{2\tau} - \frac{1}{2\varepsilon}\Big)\|v\|_0^2 - \frac{\varepsilon}{\tau}(u^{m-1}, v) \\ &= \mathcal{E}(v) + \frac{\varepsilon}{2\tau}\|v\|_0^2 - \frac{|\Omega|}{2\varepsilon} - \frac{\varepsilon}{\tau}(u^{m-1}, v) \end{aligned}$$

if $\tau \leq \varepsilon^2$. Note that $\mathcal{J}$ is convex in this case and strictly convex for $\tau < \varepsilon^2$. This immediately leads to the following existence result.

Proposition 3.1. *Let $\tau < \varepsilon^2$. Then the spatial problem* (3.1) *has a unique solution u^m for all $m = 1, \dots, M$.*

Proof. As $\mathcal{J}$ is strictly convex, lower semicontinuous, and, by

$$\mathcal{J}(v) \geq \Big(\inf_{|x|=1} \gamma(x)\Big)^2 \frac{\varepsilon}{2}\|\nabla v\|_0^2 + \Big(\frac{\varepsilon}{2\tau} - \frac{1}{2\varepsilon}\Big)\|v\|_0^2 - \frac{\varepsilon}{\tau}(u^{m-1}, v),$$

coercive for $\tau < \varepsilon^2$, existence and uniqueness follows from Proposition 1.2 in [13, Chapter II]). □

We now concentrate on stability.

Proposition 3.2. *Let $\tau < \varepsilon^2$. Then the Ginzburg–Landau free energy $\mathcal{E}$ defined in* (2.1) *is a Lyapunov functional for* (3.1) *satisfying*

$$\frac{\varepsilon}{2\tau}\|u^m - u^{m-1}\|_0^2 + \frac{\varepsilon\mu}{4}\|\nabla u^m - \nabla u^{m-1}\|_0^2 + \mathcal{E}(u^m) \le \mathcal{E}(u^{m-1}). \tag{3.2}$$

Proof. Inserting $v = u^{m-1}$ into (3.1) and exploiting (2.10) we get

$$\begin{aligned}\frac{\varepsilon}{\tau}\|u^m - u^{m-1}\|_0^2 \le \left\langle \nabla \mathcal{J}_0(u^m), u^{m-1} - u^m \right\rangle + \frac{1}{\varepsilon}\psi(u^{m-1}) - \frac{1}{\varepsilon}\psi(u^m) \\ + \frac{1}{\varepsilon}\left(\frac{1}{2}\|u^{m-1}\|_0^2 - \frac{1}{2}\|u^m\|_0^2 - (u^m, u^{m-1} - u^m)\right).\end{aligned}$$

The binomial formula $-2a(b-a) = a^2 + (b-a)^2 - b^2$ yields

$$-(u^m, u^{m-1} - u^m) = \frac{1}{2}\|u^m\|_0^2 + \frac{1}{2}\|u^m - u^{m-1}\|_0^2 - \frac{1}{2}\|u^{m-1}\|_0^2.$$

Together with the strong convexity of $\mathcal{J}_0$ as stated in Corollary 2.2 this implies

$$\begin{aligned}\left(\frac{\varepsilon}{\tau} - \frac{1}{2\varepsilon}\right)\|u^m - u^{m-1}\|_0^2 &\le \left\langle \nabla \mathcal{J}_0(u^m), u^{m-1} - u^m \right\rangle + \frac{1}{\varepsilon}\psi(u^{m-1}) - \frac{1}{\varepsilon}\psi(u^m) \\ &\le \mathcal{E}(u^{m-1}) - \mathcal{E}(u^m) - \frac{\varepsilon\mu}{4}\|\nabla(u^m - u^{m-1})\|_0^2.\end{aligned}$$

Now the equivalence of $\tau < \varepsilon^2$ and $\frac{\varepsilon}{\tau} - \frac{1}{2\varepsilon} > \frac{\varepsilon}{2\tau}$ provides the assertion. □

Now we are ready to state the main result of this section.

Theorem 3.1. *The fully implicit Euler method* (3.1) *is conditionally stable in the sense that*

$$\frac{\varepsilon}{2\tau}\sum_{m=1}^{M}\|u^m - u^{m-1}\|_0^2 + \frac{\varepsilon\mu}{4}\sum_{m=1}^{M}\|\nabla u^m - \nabla u^{m-1}\|_0^2 \le \mathcal{E}(u^0). \tag{3.3}$$

holds for all $\tau < \varepsilon^2$.

Proof. Using the estimate in Proposition 3.2 with $m = 1, \dots, M$ and $\mathcal{E}(v) \ge 0$ yields the assertion. □

As a by-product of Proposition 3.2 we get

$$\mathcal{J}_0(u^m) \le \mathcal{E}(u^m) \le \mathcal{E}(u^{m-1}) \le \cdots \le \mathcal{E}(u^0)$$

providing the following variant of (3.3)

$$\begin{aligned}\frac{\varepsilon}{2\tau}\sum_{m=1}^{M}\|u^m - u^{m-1}\|_0^2 + \frac{\varepsilon\mu}{4}\sum_{m=1}^{M}\|\nabla u^m - \nabla u^{m-1}\|_0^2 \\ + \max_{m=0,\dots,M}\mathcal{J}_0(u^m) \le 2\mathcal{E}(u^0)\end{aligned}$$

which also holds for $\tau < \varepsilon^2$.

3.2. **Semi-implicit nonlinear Euler method.** According (2.10) the double–well potential ψ consists of the convex part ϕ, the concave part $-\|\cdot\|_0^2$, and a constant. Explicit discretization of the concave part leads to the semi-implicit Euler method

$$u^m \in H^1(\Omega): \quad \frac{\varepsilon}{\tau}(u^m - u^{m-1}, v - u^m) + \langle \nabla \mathcal{J}_0(u^m), v - u^m \rangle + \frac{1}{\varepsilon}\big(\phi(v) - \phi(u^m)\big) \geq \frac{1}{\varepsilon}(u^{m-1}, v - u^m) \qquad \forall v \in H^1(\Omega). \tag{3.4}$$

We first state existence and uniqueness.

Proposition 3.3. *For all $\tau > 0$ the spatial problem* (3.4) *has a unique solution u^m for all $m = 1, \dots, M$.*

Proof. The variational inequality (3.4) is equivalent to a minimization problem for the energy

$$\mathcal{J}(v) = \mathcal{J}_0(v) + \frac{1}{\varepsilon}\phi(v) + \frac{\varepsilon}{2\tau}\|v\|_0^2 - \Big(\frac{\varepsilon}{\tau} + \frac{1}{\varepsilon}\Big)(u^{m-1}, v).$$

As $\mathcal{J}$ is strictly convex, lower semicontinuous and coercive for all $\tau > 0$ the assertion follows from Proposition 1.2 in [13, Chapter II]). □

We now show that semi-implicit Euler method (3.4) is unconditionally stable.

Theorem 3.2. *For all $\tau > 0$ the Ginzburg–Landau free energy $\mathcal{E}$ defined in* (2.1) *is a Lyapunov functional for* (3.4) *satisfying*

$$\left(\frac{\varepsilon}{\tau} + \frac{1}{2\varepsilon}\right)\|u^m - u^{m-1}\|_0^2 + \frac{\varepsilon\mu}{4}\|\nabla u^m - \nabla u^{m-1}\|_0^2 + \mathcal{E}(u^m) \leq \mathcal{E}(u^{m-1}). \tag{3.5}$$

The semi-implicit Euler method (3.4) *is unconditionally stable in the sense that*

$$\left(\frac{\varepsilon}{\tau} + \frac{1}{2\varepsilon}\right)\sum_{m=1}^{M}\|u^m - u^{m-1}\|_0^2 + \frac{\varepsilon\mu}{4}\sum_{m=1}^{M}\|\nabla u^m - \nabla u^{m-1}\|_0^2 \leq \mathcal{E}(u^0) \tag{3.6}$$

holds for all $\tau > 0$.

Proof. To show (3.5) we can almost literally repeat the proof of (3.2). However, the mixed term now takes the form

$$-(u^{m-1}, u^{m-1} - u^m) = \frac{1}{2}\|u^m\|_0^2 - \frac{1}{2}\|u^m - u^{m-1}\|_0^2 - \frac{1}{2}\|u^{m-1}\|_0^2.$$

The stability estimate (3.6) then follows as in the proof of Theorem 3.1. □

4. Linearized time discretization

4.1. **Fully implicit linearized Euler method.** In order to avoid the nonlinear term $(\gamma^2)'(\nabla u^m)$ in $\nabla \mathcal{J}_0(u^m)$ occurring in the spatial problems (3.1) and (3.4), respectively, we use, inspired by Taylor expansion, the linear approximation

$$\langle \nabla \mathcal{J}_0(u^m), v\rangle \approx \big\langle \nabla \mathcal{J}_0(u^{m-1}), v\big\rangle + \varepsilon\lambda\big(\nabla(u^m - u^{m-1}), \nabla v\big) \tag{4.1}$$

with suitable $\lambda > 0$. Here $\varepsilon\lambda(\nabla\cdot, \nabla\cdot)$ plays the role of the derivative of $\nabla \mathcal{J}_0(u^{m-1})$ which is in general does not exist, because $(\gamma^2)''(x)$ is not defined in $x = 0$. Inserting

the approximation (4.1) into (3.1), we obtain the fully implicit linearized Euler method

$$u^m \in H^1(\Omega): \tag{4.2}$$

$$\frac{\varepsilon}{\tau}(u^m - u^{m-1}, v - u^m) + \varepsilon\lambda(\nabla u^m, \nabla(v - u^m)) + \frac{1}{\varepsilon}(\phi(v) - \phi(u^m)) - \frac{1}{\varepsilon}(u^m, v - u^m)$$
$$\geq \varepsilon\lambda(\nabla u^{m-1}, \nabla(v - u^m)) - \left\langle \nabla \mathcal{J}_0(u^{m-1}), v - u^m \right\rangle \qquad \forall v \in H^1(\Omega).$$

Existence follows by the same arguments as in Proposition 3.1.

Proposition 4.1. *Let $\tau < \varepsilon^2$, $\lambda > 0$, and $u^0 \in H^1(\Omega)$. Then the spatial problem (4.2) has a unique solution u^m for all $m = 1, \ldots, M$.*

We now investigate stability.

Theorem 4.1. *Let $\tau < \varepsilon^2$ and choose $\lambda \geq L/2$. Then the Ginzburg–Landau free energy $\mathcal{E}$ defined in (2.1) is a Lyapunov functional for (4.2) satisfying*

$$\frac{\varepsilon}{2\tau}\|u^m - u^{m-1}\|_0^2 + \frac{\varepsilon\mu}{4}\|\nabla u^m - \nabla u^{m-1}\|_0^2 + \mathcal{E}(u^m) \leq \mathcal{E}(u^{m-1}). \tag{4.3}$$

The linearized fully implicit Euler method (4.2) is conditionally stable in the sense that

$$\frac{\varepsilon}{2\tau}\sum_{m=1}^{M}\|u^m - u^{m-1}\|_0^2 + \frac{\varepsilon\mu}{4}\sum_{m=1}^{M}\|\nabla u^m - \nabla u^{m-1}\|_0^2 \leq \mathcal{E}(u^0) \tag{4.4}$$

holds under the above assumptions.

Proof. By the same arguments as used in Proposition 3.2 we find

$$\left(\frac{\varepsilon}{\tau} - \frac{1}{2\varepsilon}\right)\|u^m - u^{m-1}\|_0^2 + \varepsilon\lambda\|\nabla u^m - \nabla u^{m-1}\|_0^2$$
$$\leq \frac{1}{\varepsilon}\psi(u^{m-1}) - \frac{1}{\varepsilon}\psi(u^m) + \left\langle \nabla \mathcal{J}_0(u^{m-1}), u^{m-1} - u^m \right\rangle.$$

By monotonicity and Lipschitz continuity of $\nabla \mathcal{J}_0$ (cf. Corollary 2.2 and 2.3), the last term can be bounded according to

$$\left\langle \nabla \mathcal{J}_0(u^{m-1}), u^{m-1} - u^m \right\rangle \leq \frac{\varepsilon L}{2}\|\nabla u^{m-1} - \nabla u^m\|_0^2 + \left\langle \nabla \mathcal{J}_0(u^m), u^{m-1} - u^m \right\rangle.$$

Using again the strong convexity of $\nabla \mathcal{J}_0$ (cf. Corollary 2.2) we get

$$\frac{\varepsilon}{2\tau}\|u^m - u^{m-1}\|_0^2 + \varepsilon\left(\frac{\mu}{4} + \lambda - \frac{L}{2}\right)\|\nabla u^m - \nabla u^{m-1}\|_0^2 + \mathcal{E}(u^m) \leq \mathcal{E}(u^{m-1}).$$

This proves (4.3). Now the stability estimate (4.4) follows as in the proof of Theorem 3.1. □

4.2. **Semi-implicit linearized Euler method.** Taking the concave term $-\|\cdot\|_0^2$ occurring in (4.2) explicitly, we obtain the semi-implicit linearized Euler method

$$u^m \in H^1(\Omega): \tag{4.5}$$

$$\frac{\varepsilon}{\tau}(u^m - u^{m-1}, v - u^m) + \varepsilon\lambda(\nabla u^m, \nabla(v - u^m)) + \frac{1}{\varepsilon}(\phi(v) - \phi(u^m))$$
$$\geq \varepsilon\lambda(\nabla u^{m-1}, \nabla(v - u^m)) - \left\langle \nabla \mathcal{J}_0(u^{m-1}), v - u^m \right\rangle + \frac{1}{\varepsilon}(u^{m-1}, v - u^m)$$
$$\forall v \in H^1(\Omega).$$

Existence follows by the same arguments as in Proposition 3.3.

Proposition 4.2. *Let $\tau > 0$, $\lambda > 0$, and $u^0 \in H^1(\Omega)$. Then the spatial problem* (4.5) *has a unique solution u^m for all $m = 1, \dots, M$.*

Again, the semi-implicit variant is stable without any constraints on the time step.

Theorem 4.2. *Choose $\lambda \geq L/2$. Then for all $\tau > 0$ the Ginzburg–Landau free energy $\mathcal{E}$ defined in* (2.1) *is a Lyapunov functional for* (3.4) *satisfying*

$$\left(\frac{\varepsilon}{\tau} + \frac{1}{2\varepsilon}\right) \|u^m - u^{m-1}\|_0^2 + \frac{\varepsilon\mu}{4} \|\nabla u^m - \nabla u^{m-1}\|_0^2 + \mathcal{E}(u^m) \leq \mathcal{E}(u^{m-1}). \tag{4.6}$$

The semi-implicit Euler method (3.4) *is unconditionally stable in the sense that*

$$\left(\frac{\varepsilon}{\tau} + \frac{1}{2\varepsilon}\right) \sum_{m=1}^{M} \|u^m - u^{m-1}\|_0^2 + \frac{\varepsilon\mu}{4} \sum_{m=1}^{M} \|\nabla u^m - \nabla u^{m-1}\|_0^2 \leq \mathcal{E}(u^0) \tag{4.7}$$

holds for all $\tau > 0$.

Proof. The assertions follow by the arguments used in the proof of Theorem 4.1 with the mixed term handled as in the proof of Theorem 3.2. □

5. Finite element discretization of the spatial problems

For all time discretizations presented above, a stationary convex minimization problem

$$u \in H^1(\Omega) : \qquad \mathcal{J}(u) \leq \mathcal{J}(v) \qquad \forall v \in H^1(\Omega) \tag{5.1}$$

has to be solved in each time step. The convex energy always takes the form

$$\mathcal{J}(v) := \mathcal{J}_0(v) + c\|v\|_0^2 - \langle f, v\rangle + \frac{1}{\varepsilon}\phi(v)$$

where $\mathcal{J}_0$ given in (2.7) involves a functional γ satisfying Assumptions (A1) and (A2), $c > 0$ is some constant, $f \in (H^1(\Omega))'$ is a functional . Note that $\gamma = \sqrt{\lambda}|\cdot|$ is isotropic for the linearized time discretizations as introduced in Section 4 and coincides with the original anisotropy function γ in the nonlinear case (cf. Section 3).

The spatial problem (5.1) is discretized in space by piecewise linear conforming finite elements

$$\mathcal{S}(\mathcal{T}) = \{v \in C(\overline{\Omega}) \,:\, v|_e \text{ is affine } \forall e \in \mathcal{T}\}$$

on a simplicial partition $\mathcal{T}$ of Ω. We assume that $\mathcal{T} = \mathcal{T}_j$ and an underlying hierarchy $\mathcal{T}_0, \dots, \mathcal{T}_j$ are obtained by successive refinement of a conforming intentionally coarse partition $\mathcal{T}_0$. Note that $\mathcal{T}_0$ and thus $\mathcal{T}$ might involve so-called "hanging nodes" on edge mid points. The conforming nodal basis of $\mathcal{S}(\mathcal{T})$ is denoted by λ_p, $p \in \mathcal{N}(\mathcal{T})$, where $\mathcal{N}(\mathcal{T})$ is the set of non-hanging nodes in $\mathcal{T}$. For a precise definition of hanging nodes and the conforming nodal basis we refer to [19]. The approximate nonsmooth nonlinear functional $\phi_{\mathcal{T}}$,

$$\phi_{\mathcal{T}}(v) = \sum_{p \in \mathcal{N}(\mathcal{T})} \Phi(v(p)) \int_\Omega \lambda_p(x)\, dx,$$

is obtained by replacing exact integration by a quadrature rule based on nodal interpolation in $\mathcal{S}(\mathcal{T})$.

This leads to the discrete minimization problem

$$u_{\mathcal{T}} \in \mathcal{S}(\mathcal{T}): \qquad \mathcal{J}_{\mathcal{T}}(u_{\mathcal{T}}) \le \mathcal{J}_{\mathcal{T}}(v) \qquad \forall v \in \mathcal{S}(\mathcal{T}) \tag{5.2}$$

for the discretized energy

$$\mathcal{J}_{\mathcal{T}}(v) := \mathcal{J}_0(v) + c\|v\|_0^2 - \langle f, v\rangle + \frac{1}{\varepsilon}\phi_{\mathcal{T}}(v).$$

Note that (5.2) can be equivalently rewritten in terms of coefficient vectors $U, V \in \mathbb{R}^n$ of $u, v \in \mathcal{S}(\mathcal{T})$ with respect to the nodal basis. Then the discretized spatial problems take the form problems

$$U \in \mathbb{R}^n: \qquad J(U) \le J(V) \qquad \forall V \in \mathbb{R}^n \tag{5.3}$$

with

$$J(V) = \mathcal{J}_{\mathcal{T}}\Big(\sum_{i=1}^n V_i \lambda_{p_i}\Big) = J_0(V) + \sum_{i=1}^n \varphi_i(V_i).$$

Here we used

$$J_0(V) = \Big(\mathcal{J}_0 + c\|\cdot\|_0^2 + \langle f, \cdot\rangle\Big)\Big(\sum_{i=1}^n V_i \lambda_{p_i}\Big), \qquad \varphi_i(z) = \frac{1}{\varepsilon}\Phi(z)\int_\Omega \lambda_{p_i}(x)\,dx$$

and a fixed enumeration $\mathcal{N}(\mathcal{T}) = \{p_1, \dots, p_n\}$. For the iterative solution of large-scale highly nonlinear algebraic problems of the form (5.3) by *truncated nonsmooth Newton methods* (TNNMG) we refer to [18, 19, 20].

6. Numerical experiments

6.1. **A 2D model problem.** In this section, we investigate the accuracy and numerical complexity of nonlinear time discretizations NONLIN and NONLIN-SEMI introduced in Sections 3.1 and 3.2 and the linearized variants LIN(λ) and LINSEMI(λ) introduced in Sections 4.1 and 4.2, respectively. To this end, we consider the anisotropic mean curvature flow of $\Gamma(0) = \{x \in \mathbb{R}^2 \mid \gamma^*(x) = r\}$. In this case, the solution

$$\Gamma(t) = \{x \in \mathbb{R}^2 \mid \gamma^*(x) = \sqrt{r^2 - 2t}\}, \quad 0 \le t \le r^2/2,$$

is explicitly known [16, Theorem 1.7.3].

6.1.1. *Accuracy.* Assuming that the deviation from the exact solution is dominated by the discretization error and not by the modeling error due to phase field approximation, the exact radius $r(t) = \sqrt{r^2 - 2t}$ of $\Gamma(t)$ is compared with the approximations provided by our time discretizations. In our first experiment, we select the Kobayashi anisotropy $\gamma_{k,\bar a}$ with $k = 3$ and $\bar a = 0.124$ (cf. Example 2.1) and $r \approx 0.7958$. Note that $L/2 \approx 1.745$ (cf. (2.6)) in this case. The corresponding Wulff shape $\Gamma(0) \subset \Omega = (-1, 1)^2$ is depicted in the left picture of Figure 2.1. We consider the phase field approximation of the form (2.11) with obstacle potential Φ_0 given in (2.5) and $\varepsilon = 4 \cdot 10^{-2}$. The spatial discretization is based on a uniform triangular grid $\mathcal{T}$ with mesh size $h = \sqrt{2} \cdot 2^{-7}$. Note that $\varepsilon/h \approx 3.6$. We select the uniform time step size $\tau = 10^{-4} < \varepsilon^2$.

The exact radius $r(t)$ of $\Gamma(t)$ together with the resulting approximations over time t is depicted in Figure 6.1. The left picture shows the fully implicit schemes NONLIN and LIN(λ) for $\lambda = 0.7, 0.9, 2$. While NONLIN can hardly be distinguished from the exact solution, the accuracy of LIN(λ) strongly depends on the selection of λ. For

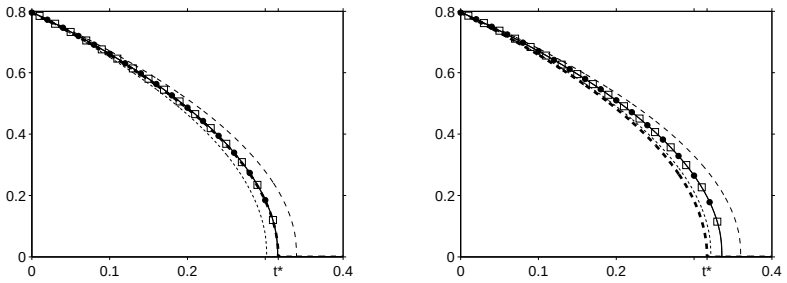

FIGURE 6.1. Radius evolutions over t for $\gamma = \gamma_{k,\bar{a}}$, $k = 3$, $\bar{a} = 0.124$. Left: Fully implicit discretizations NONLIN (-●-), LIN(λ) with $\lambda = 0.7$ (dotted), $\lambda = 0.9$ (⊟) and $\lambda = 2.0$ (dashed), and $r(t)$ (thick dashed). Right: Corresponding semi-implicit versions.

$\lambda = 0.7 < L/4$ LIN(λ) produces unstable approximations with too fast dynamics, the extinction time $t^* = r^2/2$ is approximated very well for $\lambda = 0.9 \approx L/4$, and is considerably overestimated for larger λ such as $\lambda = 2$. We emphasize that $\lambda = 0.9$ seems to provide stable solutions. This indicates that the theoretical threshold $L/2$ stated in Theorem 4.1 is not sharp. On the right, we illustrate the accuracy of the semi-implicit counterparts NONLINSEMI and LINSEMI(λ) for $\lambda = 0.7, 0.9, 2$. Though the picture looks similar at first glance, the dynamics is now slowed down by a common factor of about 0.94. This factor seems to tend to 1.0 as τ tends to 0.

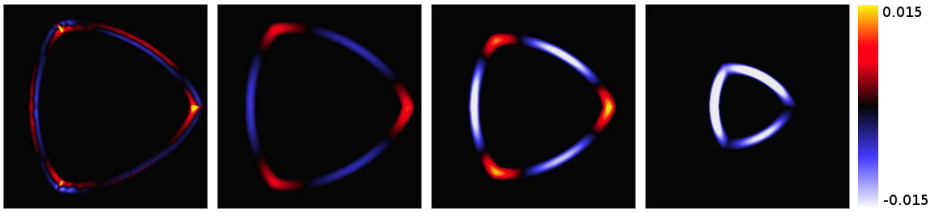

FIGURE 6.2. Difference of approximations by NONLIN and LIN(0.9) at time $t = 10^{-3}, 2 \cdot 10^{-2}, 10^{-1}, 2.5 \cdot 10^{-1}$

Figure 6.2 illustrates the smoothing effect of linearization by showing the difference of the approximations produced by NONLIN and LIN(λ) with optimal $\lambda = 0.9$, respectively. Initially, large deviations occur at the vertices which are better resolved by the anisotropic nonlinearity than by the isotropic counterpart $\lambda(\nabla\cdot, \nabla\cdot)$. It seems that these differences are smeared out but uniformly remain bounded in course of the evolution.

In the second experiment, we repeat our accuracy test for the regularized ℓ^1-norm (cf. Example 2.2) with $\mathtt{E} = 10^{-3}$. Only the two fully implicit versions are considered in this case. While, according to the left picture in Figure 6.3, NONLIN still nicely captures the evolution $r(t)$ of the sharp interface model, the linearized version LIN(λ) fails to produce any useful results: If $\lambda = 16$, 18 seems to be large enough to produce a stable discretization (though smaller than our theoretical threshold $L/2 \approx 32.6723$), then the dynamics is completely wrong. The dynamics

can be improved by smaller values $\lambda = 4$, 13, but then the discretization becomes unstable. This is illustrated by a zoom depicted in the right picture of Figure 6.3.

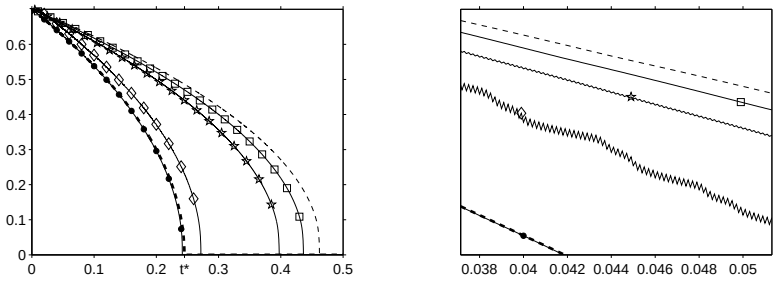

FIGURE 6.3. Radius evolutions over t for $\gamma = \gamma_{\mathrm{E}}$, $\mathrm{E} = 10^{-3}$. Left: NOLIN (-●-), LIN(λ) with $\lambda = 4.0$ (-◇-), $\lambda = 13.0$ (-⋆-), $\lambda = 16.0$ (-□-) and $\lambda = 18.0$ (dashed), and $r(t)$ (thick dashed). Right: Zoom illustrating instability of LIN(λ) for $\lambda = 4.0$ and $\lambda = 13.0$.

6.1.2. *Complexity.* While NONLIN showed high accuracy independent of any tuning parameters, the linearized version LIN(λ) is likely to require less computational effort, because the resulting spatial problems are linear in the main part of the bilinear form. In order to compare the numerical complexity of NONLIN and LIN(λ), we report the number of iteration steps and the cpu time as required by recent truncated nonsmooth Newton multigrid methods (TNNMG) [18, 19, 20] with nested iteration as applied to corresponding spatial problems. Table 1 contains these results for the first spatial problem arising from the discretization first experiment described in Section 6.1.1 with a smaller mesh size $h = \sqrt{2} \cdot 2^{-10}$ and 4 198 401 unknowns. For completeness, we also include the logarithmic potential Ψ_θ with temperature $\theta = 0.1$.

scheme	potential	iteration steps	cpu time [s]
NONLIN	obstacle	47	3694
	logarithmic	47	3034
LIN(0.9)	obstacle	8	1423
	logarithmic	32	2456

TABLE 1. Computational effort of TNNMG for a spatial problems arising from NONLIN and LIN(λ), $\lambda = 0.9$

Though the number of iteration steps is up to almost 6 times larger for NONLIN than for LIN, the gain in cpu time is less than a factor of 3, because the leading iteration steps for LIN need damping and thus are still costly. The gain in cpu time might be larger for later time steps when a diffuse interface has developed from the sharp interface in the initial condition.

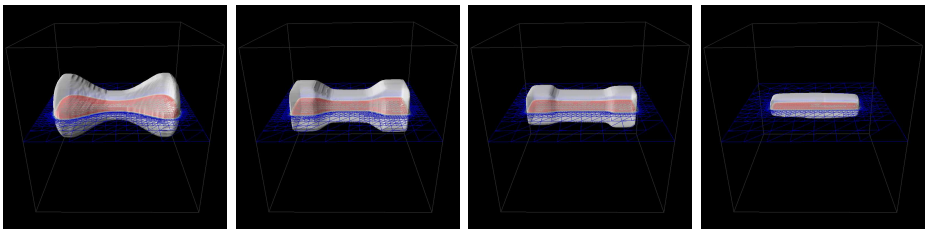

FIGURE 6.4. Evolution of dumbbell shape under anisotropic Allen–Cahn flow with regularized ℓ^1 anisotropy at $t = 4 \cdot 10^{-4}$, $6 \cdot 10^{-3}$, $1.2 \cdot 10^{-2}$, $2 \cdot 10^{-2}$

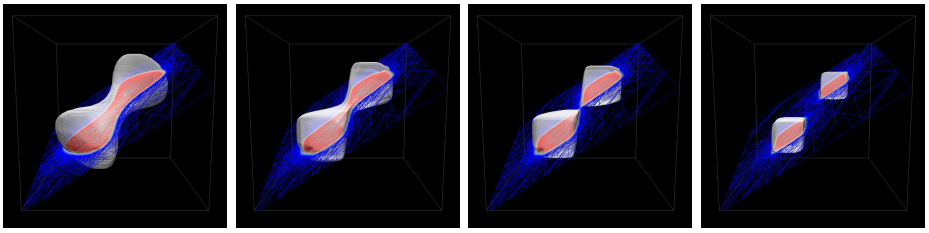

FIGURE 6.5. Evolution of dumbbell shape under anisotropic Allen–Cahn flow with regularized ℓ^1 anisotropy at $t = 4 \cdot 10^{-4}$, $6 \cdot 10^{-3}$, $9 \cdot 10^{-3}$, $1.6 \cdot 10^{-2}$

6.2. **Pinch-off in 3D.** In our final experiment, we investigate the influence of rigid body motions of the initial configuration on the occurrence of pinch-off. More precisely, we consider the dumbbell shape depicted in the left picture of Figure 6.4 and compute their anisotropic Allen–Cahn flow with obstacle potential Φ_0 given in (2.5) and $\varepsilon = 2 \cdot 10^{-2}$ with respect to the regularized ℓ^1-norm $\gamma_{\mathtt{E}}$ presented in Example 2.2. The regularization parameter is $\mathtt{E} = 10^{-3}$. Time discretization is performed by the fully implicit scheme NONLIN (cf. Section 3.1) with the time step $\tau = 2 \cdot 10^{-4} < \varepsilon^2$. The partition $\mathcal{T}$ of $\Omega = (-1, 1)^3$ is determined adaptively based on a hierarchical a posteriori error estimator [21]. In this way, small elements with minimal mesh size $h_0 = \sqrt{2} \cdot 2^{-7}$ are concentrated along the diffuse interface. The number of unknowns varies between roughly 570 000 and 14 000 during evolution from the initial time $t = 0$ to the considered final times $t = 2 \cdot 10^{-2}$ and $t = 1.6 \cdot 10^{-2}$. We emphasize that a uniform grid with mesh size h_0 would have almost 17 million unknowns that could hardly be handled on desktop computers. According to Figure 6.4 no pinch-off occurs, if the dumbbell is oriented along a coordinate axis. The situation is different, if the dumbbell is oriented along the diagonal of the coordinate system, as shown in Figure 6.5. In this case, pinch-off at $t = 8.4 \cdot 10^{-3}$ is enforced by anisotropy.

REFERENCES

[1] M. Alfaro, H. Garcke, D. Hilhorst, H. Matano, and R. Schätzle. Motion by anisotropic mean curvature as sharp interface limit of an inhomogeneous and anisotropic Allen–Cahn equation. *Proc. Roy. Soc. Edinburgh Sect. A*, 140:673–706, 2010.

[2] J.W. Barrett, H. Garcke, and R. Nürnberg. Numerical approximation of anisotropic geometric evolution equations in the plane. *IMA J. Numer. Anal.*, 28:292–330, 2008.
[3] J.W. Barrett, H. Garcke, and R. Nürnberg. A variational formulation of anisotropic geometric evolution equations in higher dimensions. *Numer. Math.*, 109:1–44, 2008.
[4] G. Bellettini and M. Paolini. Anisotropic motion by mean curvature in the context of Finsler geometry. *Hokkaido Math. J.*, 25:537–566, 1996.
[5] M. Beneš. Diffuse-interface treatment of the anisotropic mean-curvature flow. *Appl. Math.*, 48:437–453, 2003.
[6] M. Beneš. Computational studies of an anisotropic diffuse interface model of microstructure formation. *Acta Math. Univ. Comeniae*, 76:39–50, 2007.
[7] E. Burman and J. Rappaz. Existence of solutions to an anisotropic phase-field model. *Math. Meth. Appl. Sci.*, 26:1137–1160, 2003.
[8] R. Cerf. *The Wulff Crystal in Ising and Percolation Models*. Springer, 2006.
[9] K. Deckelnick and G. Dziuk. Discrete anisotropic curvature flow of graphs. *Math. Model. Numer. Anal.*, 33:1203–1222, 1999.
[10] K. Deckelnick and G. Dziuk. A fulls discrete numerical scheme for weighted mean curvature flow. *Numer. Math.*, 91:423–452, 2002.
[11] K. Deckelnick, G. Dziuk, and C.M. Elliott. Computation of geometric partial differential equations and mean curvature flow. *Acta Numerica*, 14:139–232, 2005.
[12] G. Dziuk. Discrete anisotropic curve shortening flow. *SIAM J. Numer. Anal.*, 36:1808–1830, 1999.
[13] I. Ekeland and R. Temam. *Convex Analysis and Variational Problems*. SIAM, 1999.
[14] C.M. Elliott and R. Schätzle. The limit of the anisotropic double-obstacle Allen–Cahn equation. *Proc. Roy. Soc. Edinburgh Sect. A*, 126:1217–1234, 1996.
[15] C.M. Elliott and R. Schätzle. The limit of the fully anisotropic double-obstacle Allen–Cahn equation in the nonsmooth case. *SIAM J. Math. Anal.*, 28:274–303, 1997.
[16] Y. Giga. *Surface Evolution Equations*. Birkhäuser, Basel, 2006.
[17] H. Gracke, B. Nestler, and B. Stoth. Anisotropy in multiphase sytems: a phase-field approach. *Interfaces Free Bound.*, 1:175–198, 1999.
[18] C. Gräser. Truncated nonsmooth monotone multigrid methods for anisotropic variational problems. To appear.
[19] C. Gräser. *Convex Minimization and Phase Field Models*. PhD thesis, Freie Universität Berlin, 2011.
[20] C. Gräser and R. Kornhuber. Multigrid methods for obstacle problems. *J. Comp. Math.*, 27(1):1–44, 2009.
[21] Carsten Gräser, Ralf Kornhuber, and Uli Sack. On hierarchical error estimators for time-discretized phase field models. In G. Kreiss, P.Lötstedt, A. Malqvist, and M. Neytcheva, editors, *Proceedings of ENUMATH 2009*, pages 397–406. Springer, 2010.
[22] R. Kobayashi. Modeling and numerical simulations of dendritic crystal growth. *Physica D*, 63:410–423, 1993.
[23] M. Paolini. Fattening in two dimensions obtained with a non-symmetric anisotropy: numerical simulations. *Acta Math. Univ. Comeniae*, 67:43–55,

1998.

[24] P. Pozzi. Anisotropic mean curvature flow for two dimensional surfaces in higher codimension: a numerical scheme. *Interfaces Free Bound.*, 10:539–576, 2008.

[25] G. Wulff. Zur Frage der Geschwindigkeit des Wachstums und der Auflšung von Krystallflchen. *Zeitschrift fur Krystallographie und Mineralogie*, 34:449–530, 1901.

Carsten Gräser, Freie Universität Berlin, Institut für Mathematik, Arnimallee 6, D - 14195 Berlin, Germany

E-mail address: graeser@math.fu-berlin.de

Prof. Dr. Ralf Kornhuber, Freie Universität Berlin, Institut für Mathematik, Arnimallee 6, D - 14195 Berlin, Germany

E-mail address: kornhuber@math.fu-berlin.de

Uli Sack, Freie Universität Berlin, Institut für Mathematik, Arnimallee 6, D - 14195 Berlin, Germany

E-mail address: usack@math.fu-berlin.de